# An Adaptive hp-Version of the Multilevel Particle–Partition of Unity Method

Marc Alexander Schweitzer [1]

*Rheinische Friedrich-Wilhelms-Universität Bonn, Institut für Numerische Simulation, Wegelerstraße 6, D-53115 Bonn, Germany*

**Abstract**

This paper is concerned with the hp-adaptive multilevel solution of second order elliptic partial differential equations using the meshfree particle–partition of unity method. The proposed refinement scheme automatically constructs new discretization points (or particles), the meshfree analogue of an adaptive h-refinement, and local approximation spaces with better local resolution, a p-refinement.

The refinement process is steered with the help of an a-posteriori subdomain-type error indicator. We present results of numerical experiments in two and three space dimensions which demonstrated the overall efficiency of the proposed scheme.

*Key words:* keywords
*1991 MSC:* MSC-NUMBERS

## 1 Introduction

Meshfree methods (MM) are promising tools for the numerical solution of partial differential equations (PDE) in complex large scale engineering applications since they are based on a finite collection of (independent) points only and do not require the use of a computational mesh as the finite element method (FEM). Hence, an adaptive refinement process in meshfree methods does not have to deal with the cumbersome task of mesh-refinement but merely with the generation of new independent points and the selection of independent local approximation spaces. The flexibility and robustness of MM

*Email address:* schweitzer@ins.uni-bonn.de (Marc Alexander Schweitzer).
*URL:* wissrech.ins.uni-bonn.de/people/schweitz.html (Marc Alexander Schweitzer).

[1] Sonderforschungsbereich 611

make them very attractive approaches in a wide range of applications, e.g. large deformation analysis, crack propagation, fluid dynamics, astrophysics and magneto-hydrodynamics and many more, see [21, 22, 24, 26] and the references therein. However, these benefits come at a price. MM are in general somewhat more involved than classical finite element schemes for instance with respect to numerical integration [1, 5, 9–11, 18, 33], the implementation of essential boundary conditions [1, 20, 26, 27], and the linear independence of the employed shape functions [36, 39, 40]. The latter issue also complicates the efficient solution of the arising linear systems. Classical fast solvers like multigrid [25, 45] are not directly applicable in MM but rather have to be modified in an appropriate way [16, 19]. Hence, the design and implementation of an efficient and stable meshfree solver is a challenging task and the number of codes applicable to large scale problems is rather small.

In this paper we focus on the particle–partition of unity method (PPUM) [17, 36]. The PPUM is a meshfree generalized finite element method based on the partition of unity (PU) approach developed in [2, 3, 15] but employs a so-called flat top PU to ensure that the constructed shape functions are linearly independent. A PPUM shape function $\varphi_i \psi_i^k$ is a product of a PU function $\varphi_i$ and an approximation function $\psi_i^k$. The PU function provides the locality and the compact support of the shape function, whereas the function $\psi_i^k$ provides the approximation properties on $\omega_i = \text{supp}(\varphi_i)$. Hence, we refer to the PU functions $\varphi_i$ as the h-components and the $\psi_i^k$ are denoted p-components. Note however that we are not restricted to the use of classical polynomials as approximation functions $\psi_i^k$. One of the key-benefits of the PU framework is that we can use problem-dependent approximation functions to improve the overall efficiency of the method. If, for instance, a particular (local) behavior of the solution is know a-priori (e.g. by asymptotic analysis in the vicinity of a crack tip) this information can easily be incorporated in the PPUM approximation space by adding special enrichment functions $\zeta_i^m$ to the approximation, i.e., including the functions $\varphi_i \zeta_i^m$ in the basis.

If however no analytic enrichment information is available or only of low quality, then the functions $\zeta_i^m$ must be constructed numerically. In principal $\zeta_i^m$ can be computed using the FEM or other grid-based techniques. With such a classical numerical scheme however the utilization of previously computed special functions in an efficient self-adaptive approximation process is not feasible. Hence, we suggest the use of the PPUM also for the computation of special enrichment functions. Such enrichment functions are obviously discontinuous or singular functions—otherwise the direct use of classical polynomials is already sufficient. Therefore, the efficient approximation of such enrichment functions requires an adaptive numerical procedure. To this end, we have developed an h-adaptive version of our multilevel PPUM in [23]. In this paper we now extend these results to an hp-adaptive approach.

The remainder of the paper is organized as follows. In §2 we shortly review the core ingredients of the PPUM and the implementation of essential boundary conditions in the PPUM. Then, we present the employed error estimator and our refinement scheme in §3. The results of our numerical experiments are presented in §4. In particular, we consider the hp-adaptive approximation of scalar diffusion problems in two and three space dimensions and of a two-dimensional linear elastic fracture mechanics problem with analytical enrichment. The presented results clearly show the overall efficiency of the proposed scheme. Finally, we conclude with some remarks in §5.

## 2 Particle–Partition of Unity Method

In this section let us shortly review the core ingredients of the PPUM, see [18, 19, 36] for details. In a first step, we need to construct a PPUM space $V^{\mathrm{PU}}$, i.e., we need to specify the PPUM shape functions $\varphi_i\psi_i^k$. With these shape functions, we then set up a sparse linear system of equations $A\tilde{u} = \hat{f}$ via the classical Galerkin method which is then solved by a full multigrid type iterative solver [19, 23]. However, we need to employ a non-standard variational formulation of the PDE to account for the fact that our PPUM shape functions—like most meshfree shape functions—do not satisfy essential boundary conditions explicitly.

To specify the PPUM shape functions $\varphi_i\psi_i^k$, i.e. the PU functions $\varphi_i$, let us first introduce the notion of a cover $C_\Omega$ of a computational domain $\Omega \subset \mathbb{R}^d$, i.e., the PPUM analogue of a computational mesh.

**Definition 2.1 (Cover)** *Let $\Omega \subset \mathbb{R}^d$ be an open set. Let $\omega_i \subset \mathbb{R}^d$ be open sets with $\Omega \cap \omega_i \neq \emptyset$ for $i = 1, \ldots, N$. The collection $C_\Omega := \{\omega_i \,|\, i = 1, \ldots, N\}$ is called a cover of $\Omega$ and the sets $\omega_i$ cover patches if the following conditions are satisfied.*

- *Global covering:*

$$\overline{\Omega} \subset \bigcup_{i=1}^{N} \omega_i.$$

- *Bounded overlap: The mapping $\lambda_{C_\Omega} : \overline{\Omega} \to \mathbb{N}$ such that*

$$\lambda_{C_\Omega}(x) = \mathrm{card}\{\omega_j \in C_\Omega \,|\, x \in \omega_i\}$$

*denotes the associated covering index. There exists a constant $\hat{M} > 0$ such that for any $x \in \Omega$ there holds*

$$\|\lambda_{C_\Omega}\|_{L^\infty(\Omega)} < \hat{M} \ll N. \tag{1}$$

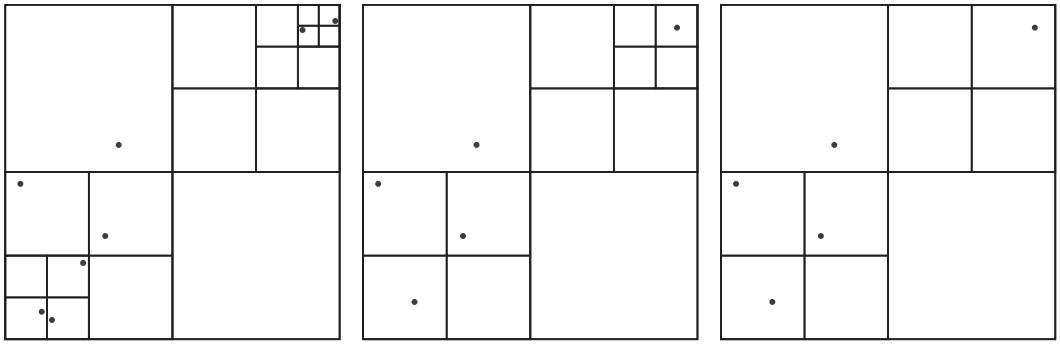

Figure 1. Subdivision corresponding to a cover on level $J = 4$ with initial point cloud (left), derived coarser subdivisions on level 3 (center), and level 2 (right) with respective coarser point cloud.

- *Sufficient overlap: There exists a constant $K > 0$ such that for any $x \in \Omega$ there is at least one cover patch $\omega_i$ such that $x \in \omega_i$ and*

$$\operatorname{dist}(x, \partial\omega_i) \geq K \operatorname{diam}(\omega_i). \tag{2}$$

- *Comparability of neighboring patches: A subset*

$$C_{\Omega,i} := \{\omega_j \in C_\Omega \,|\, \omega_j \cap \omega_i \neq \emptyset\} \subset C_\Omega \tag{3}$$

*is called a local neighborhood or local cover of a particular cover patch $\omega_i \in C_\Omega$. There exist constants $C_L > 0$ and $C_U > 0$ such that for all local neighborhoods $C_{\Omega,i}$ there holds the implication*

$$\omega_j \in C_{\Omega,i} \quad \Rightarrow \quad C_L \operatorname{diam}(\omega_i) \leq \operatorname{diam}(\omega_j) \leq C_U \operatorname{diam}(\omega_i). \tag{4}$$

In [18,19] we have developed a tree-based cover construction scheme that gives a multilevel sequence of covers $\{C_\Omega^k\}$ with $k = 1, \ldots, J$ based on a given point set $P = \{x_i \,|\, i = 1, \ldots, \hat{N}\}$. The fundamental construction principle employed in [18] is a $d$-binary tree. Based on the given point data $P = \{x_i \,|\, i = 1, \ldots, \hat{N}\}$, we sub-divide a bounding-box $\mathcal{C}_\Omega \supset \Omega$ until each cell

$$\mathcal{C}_i = \prod_{l=1}^{d} (c_i^l - h_i^l, c_i^l + h_i^l)$$

associated with a leaf of the tree contains at most a single point $x_i \in P$, see Figure 1 (left). We obtain a valid cover from this tree by defining the cover patches by

$$\omega_i := \prod_{l=1}^{d} (c_i^l - \alpha h_i^l, c_i^l + \alpha h_i^l), \quad \text{with } \alpha > 1. \tag{5}$$

Note that we define a cover patch $\omega_i$ for leaf-cells $\mathcal{C}_i$ that contain a point $x_i \in P$ as well as for *empty* cells that do not contain any point from $P$. The coarser covers $C_\Omega^k$ are defined considering coarser versions of the constructed

tree, i.e., by removing a complete set of leaves of the tree, see Figure 1. For details of this construction see [18, 19, 36].

To obtain a PU on a cover $C_\Omega^k$ we define a weight function $W_{i,k} : \bigcup_{i=1}^{N_k} \omega_{i,k} \to \mathbb{R}$ with $\text{supp}(W_{i,k}) = \omega_{i,k}$ for each cover patch $\omega_{i,k}$ by

$$W_{i,k}(x) = \begin{cases} \mathcal{W} \circ T_{i,k}(x) & x \in \omega_{i,k} \\ 0 & \text{else} \end{cases} \tag{6}$$

with the affine transforms $T_{i,k} : \overline{\omega}_{i,k} \to [-1,1]^d$ and $\mathcal{W} : [-1,1]^d \to \mathbb{R}$ the reference $d$-linear B-spline. By simple averaging of these weight functions we obtain the functions

$$\varphi_{i,k}(x) := \frac{W_{i,k}(x)}{S_{i,k}(x)}, \text{ with } S_{i,k}(x) := \sum_{\omega_{j,k} \in C_{\Omega,i}^k} W_{j,k}(x) = \sum_{l=1}^{N_k} W_{l,k}(x). \tag{7}$$

We refer to the collection $\{\varphi_{i,k}\}$ with $i = 1, \ldots, N_k$ as a partition of unity since there hold the relations

$$\begin{aligned} 0 \;\le\; \varphi_{i,k}(x) \le 1, \qquad & \sum_{i=1}^{N_k} \varphi_{i,k} \equiv 1 \text{ on } \overline{\Omega}, \\ \|\varphi_{i,k}\|_{L^\infty(\mathbb{R}^d)} \le C_{\infty,k}, \qquad & \|\nabla \varphi_{i,k}\|_{L^\infty(\mathbb{R}^d)} \le \frac{C_{\nabla,k}}{\text{diam}(\omega_{i,k})} \end{aligned} \tag{8}$$

with absolute constants $0 < C_{\infty,k} < 1$ and $C_{\nabla,k} > 0$ so that the assumptions on the PU for the error analysis given in [3] are satisfied by our PPUM construction.

In general the p-components $\psi_{i,k}^n$ associated with a particular patch $\omega_{i,k}$ of a PPUM approximation space $V_k^{\text{PU}}$ are products of univariate Legendre polynomials, i.e., the global space $V_k^{\text{PU}}$ is defined as

$$V_k^{\text{PU}} := \sum_{i=1}^{N} \varphi_{i,k} V_{i,k}^{p_{i,k}}, \text{ where } V_{i,k}^{p_{i,k}}(\omega_{i,k}) := \mathcal{P}^{p_{i,k}} \circ T_{i,k}$$

$$\mathcal{P}^{p_{i,k}}((-1,1)^d) := \text{span}\langle \{\psi^n \mid \psi^n(x) = \prod_{l=1}^{d} \mathcal{L}^{\hat{n}_l}(x^l), \|\hat{n}\|_1 = \sum_{l=1}^{d} \hat{n}_l \le p_{i,k}\} \rangle,$$

where $\mathcal{L}^m$ denotes the univariate Legendre polynomial of degree $m$. [2]

Note that the relations (8) do not ensure the linear independence of the re-

[2] Note that there is no restriction on the choice of the employed norm. The use of anisotropic spaces or more general subspaces is possible in the PPUM.

sulting product functions $\psi_{i,k}\psi_{i,k}^n$ [3, 35, 39, 40], i.e., in general

$$\sum_{i=1}^{N_k} \varphi_{i,k}(x) \sum_{n=1}^{\dim V_{i,k}^{p_{i,k}}} u_{i,k}^n \psi_{i,k}^n(x) = 0 \text{ for all } x \quad \not\Rightarrow \quad u_{i,k}^n = 0 \text{ for all } (i,n).$$

A linearly independent set of product functions $\varphi_{i,k}\psi_{i,k}^n$, however, is obtained if the considered PU has the flat top property.

**Definition 2.2 (Flat top property)** *Let $\{\varphi_i\}$ be a partition of unity on the cover $C_\Omega = \{\omega_i \,|\, i = 1, \dots, N\}$. Define the sub-patches*

$$\omega_{\mathrm{FT},i} := \{x \,|\, \lambda_{C_\Omega}(x) = 1\} \text{ such that } \varphi_i|_{\omega_{\mathrm{FT},i}} \equiv 1.$$

*Then, the PU is said to have the flat top property, if there exists a constant $C_{\mathrm{FT}}$ such that for all patches $\omega_i \in C_\Omega$*

$$\mu(\omega_i) \leq C_{\mathrm{FT}}\, \mu(\omega_{\mathrm{FT},i}) \tag{9}$$

*where $\mu(A)$ denotes the Lebesgue measure of $A \subset \mathbb{R}^d$.*

If the employed local basis sets $\{\psi_{i,k}^n\}$ are linearly independent on $\omega_{\mathrm{FT},i}$ then the product functions $\varphi_{i,k}\psi_{i,k}^n$ form a stable basis of the approximation space $V_k^{\mathrm{PU}}$.

The PU (7) based on a cover $C_\Omega^k$ obtained from the scaling of a tree decomposition with $\alpha > 1$ has the flat top property if $\alpha \in (1, 1 + 2^{-L_k})$ with

$$L_k := \max_{\omega_{i,k} \in C_\Omega^k} \max_{\omega_{j,k} \in C_{\Omega,i}^k} |l_{i,k} - l_{j,k}| \tag{10}$$

and $l_{i,k}$ denotes the refinement level of the tree cell associated with $\omega_{i,k}$, see [23]. Note that the flat top property is a sufficient condition only. In practice, we obtain a linearly independent and stable set of shape functions if the flat top property is satisfied by $O(N_k)$ patches $\omega_{i,k}$ of the cover $C_\Omega^k = \{\omega_{i,k} \,|\, i = 1, \dots, N_k\}$.

The maximal level difference $L_k$ defined in (10) of a cover $C_\Omega^k$ is a measure for the irregularity of the underlying tree construction. If we enforce a global flat top property, i.e. if we use $\alpha \in (1, 1 + 2^{-L_k})$, the constants $C_{L,k}$ and $C_{U,k}$ of (4), $C_{\infty,k}$ and $C_{\nabla,k}$ of (8), and $\hat{M}$ of (1) grow with increasing $L_k$, i.e. with decreasing $\alpha$. Throughout this paper we fix the scaling parameter $\alpha = 1.3$ for all levels $k = 1, \dots, J$ and thereby enforce the flat top property on coarse levels only. On finer levels we obtain PUs which satisfy the flat top property for most but not necessarily all patches. The benefit of this approach is that the value of the constants, especially the values of $C_{\infty,k}$ and $C_{\nabla,k}$, are (almost)

independent of $L_k$ so that the irregularity of the underlying tree construction has a negligible impact on the quality of the approximation only.

With the help of the basis functions $\varphi_{i,k}\psi_{i,k}^n$ we then discretize a PDE problem in weak form

$$a(u,v) = \langle f, v \rangle$$

via the classical Galerkin method to obtain a discrete linear system of equations $A\tilde{u} = \hat{f}$. Note that the PU functions (7) in the PPUM are in general piecewise rational functions only. Therefore, the use of an appropriate numerical integration scheme is indispensable in the PPUM as in most meshfree approaches [1, 5, 10, 11, 19]. Moreover, the functions $\varphi_{i,k}\psi_{i,k}^n$ form a basis of $V_k^{\mathrm{PU}}$ but in general they do not satisfy the Kronecker property. Thus, the coefficients $\tilde{u}_k := (u_{i,k}^n)$ of a discrete function

$$u_k^{\mathrm{PU}} = \sum_{i=1}^{N_k} \varphi_i \sum_{n=1}^{\dim V_{i,k}^{p_{i,k}}} u_{i,k}^n \psi_{i,k}^n \tag{11}$$

on level $k$ do not directly correspond to function values and a trivial interpolation of essential boundary data is not available.

### *2.1 Essential Boundary Conditions*

The treatment of essential boundary conditions in meshfree methods is not straightforward and a number of different approaches have been suggested. In [20] we have presented how Nitsche's method [30] can be applied successfully in the meshfree context. Here, we give a short summary of this approach. To this end, let us consider the model problem

$$\begin{aligned} -\Delta u &= f \quad \text{in } \Omega \subset \mathbb{R}^d, \\ u &= g_D \quad \text{on } \Gamma_D \subset \partial\Omega, \\ \frac{\partial u}{\partial n} &= g_N \quad \text{on } \Gamma_N = \partial\Omega \setminus \Gamma_D. \end{aligned} \tag{12}$$

In the following we drop the level subscript $k = 1, \ldots, J$ for the ease of notation. Let $\partial_n u := \frac{\partial u}{\partial n}$ denote the normal derivative, $\Gamma_{D,i} := \omega_i \cap \Gamma_D$, $\gamma_{D,i} := \mathrm{diam}(\Gamma_{D,i})$, and

$$C_{\Gamma_D} := \{\omega_i \in C_\Omega \,|\, \Gamma_{D,i} \neq \emptyset\}$$

denotes the cover of the Dirichlet boundary.

With these conventions we define the cover-dependent functional

$$J_{C_\Omega}(w) := \int_\Omega |\nabla w|^2 - 2\int_{\Gamma_D} \partial_n w w + \beta \sum_{\omega_i \in C_{\Gamma_D}} \gamma_{D,i}^{-1} \int_{\Gamma_{D,i}} |w|^2 \tag{13}$$

with some parameter $\beta > 0$. Minimizing (13) with respect to the error $u - u^{\mathrm{PU}}$ yields the weak formulation

$$a_{C_\Omega}(w, v) = l_{C_\Omega}(v) \quad \text{for all } v \in V^{\mathrm{PU}} \tag{14}$$

with the cover-dependent bilinear form

$$a_{C_\Omega}(w, v) := \int_\Omega \nabla w \nabla v - \int_{\Gamma_D} (\partial_n w v + w \partial_n v) + \beta \sum_{\omega_i \in C_{\Gamma_D}} \gamma_{D,i}^{-1} \int_{\Gamma_{D,i}} wv \tag{15}$$

and the corresponding linear form

$$l_{C_\Omega}(v) := \int_\Omega fv - \int_{\Gamma_D} g_D \partial_n v + \int_{\Gamma_N} g_N v + \beta \sum_{\omega_i \in C_{\Gamma_D}} \gamma_{D,i}^{-1} \int_{\Gamma_{D,i}} g_D v. \tag{16}$$

There is a unique solution $u^{\mathrm{PU}}$ of (14) if the regularization parameter $\beta$ in (13) is chosen large enough; i.e., the regularization parameter $\beta = \beta_{V^{\mathrm{PU}}}$ is dependent on the discretization space $V^{\mathrm{PU}}$. This solution $u^{\mathrm{PU}}$ satisfies optimal error bounds if the space $V^{\mathrm{PU}}$ admits the following inverse estimate

$$\|\partial_n v\|_{-\frac{1}{2}, C_\Omega} \leq C_{V^{\mathrm{PU}}} \|\nabla v\|_{L^2(\Omega)} \quad \text{for all } v \in V^{\mathrm{PU}} \tag{17}$$

for the cover-dependent norm

$$\|\partial_n v\|^2_{-\frac{1}{2}, C_\Omega} := \sum_{\omega_i \in C_{\Gamma_D}} \gamma_{D,i} \|\partial_n v\|^2_{L^2(\Gamma_{D,i})}$$

with a constant $C_{V^{\mathrm{PU}}}$ depending on the cover $C_\Omega$ and the employed local bases $\{\psi_i^n\}$ only. If $C_{V^{\mathrm{PU}}}$ is known, the regularization parameter $\beta_{V^{\mathrm{PU}}}$ can be chosen as $\beta_{V^{\mathrm{PU}}} > 2C^2_{V^{\mathrm{PU}}}$ to obtain a symmetric positive definite linear system [30]. Hence, the main task associated with the use of Nitsche's approach in the PPUM context is the efficient and automatic computation of the constant $C_{V^{\mathrm{PU}}}$, see [20, 36]. To this end, we consider the inverse assumption (17) as a generalized eigenvalue problem locally on each patch $\omega_i \in C_{\Gamma_D}$ and solve for the largest eigenvalue to obtain an approximation to $C^2_{V^{\mathrm{PU}}}$.

**Remark 2.1** Due to Nitsche's approach we obtain a sequence of weak formulations (14) with level-dependent bilinear forms (15) and linear forms (16). Therefore, we also deal with a sequence of energy-norms

$$\|u\|_{A,k} := \sqrt{a_{C^k_\Omega}(u, u)}$$

with the property $\|u\|_{A,k} \leq \|u\|_{A,l}$ for $k < l$.

In summary, the PPUM discretization of our model problem (12) using the space $V^{\mathrm{PU}}$ on the cover $C_\Omega$ is carried out in two steps: First, we estimate the regularization parameter $\beta_{V^{\mathrm{PU}}}$ from (17). Then, we define the weak form (14) with (15) and (16) and use Galerkin's method to set up the respective symmetric positive definite linear system $A\tilde{u} = \hat{f}$. This linear system is then solved by our full multigrid type iterative solver [19,23]. Finally, we assess the quality of the computed approximation (11) with the help of an a-posteriori error estimation and improve the approximation efficiently using an appropriate adaptive refinement procedure.

## 3 Adaptive Refinement

In this section we present our hp-type adaptive refinement scheme. The refinement of our PPUM is steered by local error estimates defined on the overlapping cover patches $\omega_{i,J}$ on level $J$, i.e., we employ a subdomain-type error estimator [3,4,23]. In the construction of the subdomain problems, however, we have to be concerned with the fact that we employ a non-standard variational form involving a regularization parameter that depends on the discretization space. From the local estimates we obtain our refinement indicator function

$$r : C_\Omega^J \to \{\mathtt{null}, \mathtt{h}, \mathtt{p}\} \tag{18}$$

which determines the suggested refinement type for a particular patch $\omega_{i,J} \in C_\Omega^J$ on the finest level $J$. This refinement indicator uses a simple one-level history as e.g. suggested in [28] for this decision. Finally, we need to ensure that our hp-refined PPUM satisfies all the assumptions of the original PPUM construction, see §2. In the following we drop the level subscript $k$, since the adaptive refinement will always be carried out for the currently finest level $J$ of our sequence $\{V_k^{\mathrm{PU}}\}_{k=1}^J$.

### *3.1 Error Estimation*

In section 2.1 we introduced the weak formulation (14) for the treatment of the model problem (12). The bilinear form (15) and linear form (16) arise from the minimization of the functional (13) with respect to the global error $e^{\mathrm{PU}} := u - u^{\mathrm{PU}}$ for $u^{\mathrm{PU}}$ from the considered discretization space $V^{\mathrm{PU}}$, i.e

$$e^{\mathrm{PU}} = \mathrm{argmin}_{v^{\mathrm{PU}} \in V^{\mathrm{PU}}} J_{C_\Omega}(u - v^{\mathrm{PU}}).$$

Now we are interested in the local approximation of the error $e^{\mathrm{PU}}|_{\omega_i}$. To this end we consider the sequence of local problems

$$J_{C_\Omega}(e^{\mathrm{PU}}|_{\omega_i} - e_{i,*}) \to \min\{e_{i,*} \in V_{i,*}\} \tag{19}$$

for $i = 1, \ldots, N$ and the spaces $V_{i,*} := \varphi_i V_i^{p_i+q}$ which corresponds to the localized PDE

$$\begin{aligned} -\Delta e_{i,*} = -\Delta e^{\mathrm{PU}}|_{\omega_i} &= (f + \Delta u^{\mathrm{PU}})|_{\omega_i} && \text{in } \omega_i \cap \Omega \subset \mathbb{R}^d, \\ e_{i,*} = e^{\mathrm{PU}}|_{\omega_i} &= (g_D - u^{\mathrm{PU}})|_{\omega_i} && \text{on } \partial(\omega_i \cap \Omega) \setminus \Gamma_N, \\ \frac{\partial e_{i,*}}{\partial n} = \frac{\partial e^{\mathrm{PU}}|_{\omega_i}}{\partial n} &= (g_N - \frac{\partial u^{\mathrm{PU}}}{\partial n})|_{\omega_i} && \text{on } \partial(\omega_i \cap \Omega) \cap \Gamma_N, \end{aligned} \tag{20}$$

compare [3, 4, 23, 32, 43]. We discretize the terms $\Delta u^{\mathrm{PU}}$, $u^{\mathrm{PU}}$ and $\frac{\partial u^{\mathrm{PU}}}{\partial n}$ on the right-hand side of (20) by a Petrov–Galerkin approach. The current approximant $u^{\mathrm{PU}}$ is given as a linear combination of the functions $\varphi_i \psi_i^n$ from the global PPUM space $V^{\mathrm{PU}} = \sum_{i=1}^N \varphi_i V_i^{p_i}$ but the trial and test space for the discretization of (19) and (20) is $V_{i,*} = \varphi_i V_i^{p_i+q}$ with $q > 0$. The term $\Delta u^{\mathrm{PU}}$ for instance is discretized via the bilinear form (15) with the trial space $V^{\mathrm{PU}}$ and the test space $V_{i,*}$. If the PU is of higher regularity, e.g. by choosing a higher order B-spline in (6), we can also use a strong formulation.

Recall that the regularization parameter $\beta$ of (13) must be chosen with respect to the considered discretization space. Hence, for each local problem (19) we need to employ an appropriate and possibly different regularization parameter $\beta_{i,*}$ to ensure its solvability. In our implementation we use the maximal regularization parameter $\beta_{\max,*} = \max_{i=1}^N \beta_{i,*}$ for all patches. Note that the use of a larger regularization parameter overemphasizes the error distribution on the Dirichlet boundary within the energy norm. Hence it can have an adverse effect on the overall efficiency since it can lead to an unnecessary refinement near the Dirichlet boundary and it may lead to a deterioration of the convergence behavior of the iterative solver. In all our numerical experiments we found the variation in the $\beta_{i,*}$ to be small enough to avoid such an unnecessary refinement near the Dirichlet boundary.

From the local approximations $e_{i,*} \in V_{i,*}$ to the error $e^{\mathrm{PU}}$ we obtain a local estimator $\eta_{i,A}$ and a global estimate $\eta_N$ with respect to an arbitrary norm $\|\cdot\|_N$ by the definitions

$$\eta_{i,N} := \|e_{i,*}\|_{N(\omega_i \cap \Omega)}, \quad \eta_N := \Big( \sum_{i=1}^N \eta_{i,N}^2 \Big)^{1/2}. \tag{21}$$

Throughout this paper we employ the energy-norm $\|\cdot\|_{A,J}$ with respect to level $J$ for the refinement control on (the finest) level $J$, i.e., we use $\eta_i := \eta_{i,A,J}$ in the following.

To attain our refinement indicator function (18) from (21) we first define a Boolean indicator

$$b : C_\Omega \to \{\texttt{true}, \texttt{false}\}$$

by simple thresholding

$$b(\omega_i) := \begin{cases} \texttt{true} & \text{if } \eta_i \geq \sigma_b \eta_{\text{avg}}, \\ \texttt{false} & \text{else}, \end{cases}$$

with $\eta_{\text{avg}}^2 := N^{-1}\eta^2 = N^{-1}\sum_{i=1}^N \eta_i^2$ as it is done in many adaptive procedures. The second component of (18) is an assumed error reduction classifier

$$t : C_\Omega \to \{\texttt{constant}, \texttt{algebraic}, \texttt{exponential}\}$$

defined by

$$t(\omega_i) := \begin{cases} \texttt{constant} & \text{if } b(\omega_i) = \texttt{false}, \\ \texttt{algebraic} & \text{if } b(\omega_i) = \texttt{true} \text{ and } \eta_i \geq \eta_{i,*}, \\ \texttt{exponential} & \text{else}, \end{cases}$$

where $\eta_{i,*}$ is a predicted error based on the estimator $\hat{\eta}_i$ from the previous refinement step, i.e. an extrapolation of a one-level history.

If a particular patch $\omega_i$ was h-refined, i.e. $r(\omega_i) = \texttt{h}$, we anticipate that the error with respect to the energy-norm on $\omega_i$ is reduced by a factor $2^{-p_i}$. Furthermore, we assume that the error is distributed uniformly among the $2^d$ children patches, so that we predict the error on a child patch $\omega_j \subset \omega_i$ to be $\eta_{j,*} := \sigma_{\texttt{h}} 2^{-d} 2^{-p_i} \eta_i$ with $\sigma_{\texttt{h}} > 0$. In the case of a p-refined patch $\omega_i$ we anticipate an exponential convergence on $\omega_i$ and set $\eta_{i,*} := \sigma_{\texttt{p}} \eta_i$ with $0 < \sigma_{\texttt{p}} < 1$. For patches $\omega_i$ that are not refined we set $\eta_{i,*} := \sigma_{\texttt{null}} \eta_i$ with $\sigma_{\texttt{null}} > 0$ and we obtain the overall definition

$$\eta_{i,*} := \begin{cases} \sigma_{\texttt{null}} \eta_i & \text{if } t(\omega_i) = \texttt{constant}, \\ \sigma_{\texttt{p}} \eta_i & \text{if } t(\omega_i) = \texttt{exponential}, \\ \sigma_{\texttt{h}} 2^{-d} 2^{-p_j} \eta_j & \text{if } \omega_j \supset \omega_i \text{ and } t(\omega_j) = \texttt{algebraic}. \end{cases} \tag{22}$$

Obviously, this prediction assumes that the respective refinement yields an optimal error reduction. Hence, if $\eta_i < \eta_{i,*}$ the refinement reduced the error better than predicted which indicates a higher regularity of the solution and that an `exponential` convergence may be achieved on $\omega_i$. If $\eta_i \geq \eta_{i,*}$, we

assume that the smoothness of the solution $u$ is limited on $\omega_i$ and only an `algebraic` convergence is attainable.

If there is no local refinement, i.e. $r(\omega_i) = \texttt{null}$, we assume an almost `constant` error on the patch $\omega_i$ which disregards effects due to the overlap of the patches. Note however that we can account for changes to the local error due to changes to the respective PU function $\varphi_i$ stemming from the h-refinement of neighboring patches $\omega_j \in C_{\Omega,i}$ by using a local parameter $\sigma_{\texttt{null},i}$.

With these components in place, we define a completely local refinement indicator function

$$r(\omega_i) := \begin{cases} \texttt{null} \text{ if } t(\omega_i) = \texttt{constant}, \\ \texttt{h} \quad \text{if } t(\omega_i) = \texttt{algebraic}, \\ \texttt{p} \quad \text{if } t(\omega_j) = \texttt{exponential}, \end{cases} \tag{23}$$

which steers the refinement of the PPUM space $V^{\mathrm{PU}}$ defined on the cover $C_\Omega$. If $r(\omega_i) = \texttt{h}$ we refine the h-components of $V^{\mathrm{PU}}$, i.e., the PU functions $\varphi_i$. Due to our construction this essentially means that we refine the cover $C_\Omega$ by refining the respective cover patch $\omega_i$. This is accomplished by the introduction of new particles $\xi \in \omega_i$, see [23] for the details of the employed particle creation scheme. The refinement of the p-components in the case of $r(\omega_i) = \texttt{p}$ is straightforward, we simply increase the current polynomial degree $p_i$ on $\omega_i$ by one.

Note that this refinement scheme generates a new level $J+1$ for our multilevel sequence only if the refinement indicator $r(\omega_{i,J}) = \texttt{h}$ for a particular patch $\omega_{i,J}$ that satisfies

$$\omega_{i,J} \in C_\Omega^J \text{ and } \omega_{i,J} \notin C_\Omega^k \text{ for all } k = 1, \ldots, J-1.$$

If there is no such patch $\omega_{i,J}$ the current space $V_J^{\mathrm{PU}}$ is replaced by its refined version.

**Remark 3.1** With the presented refinement scheme there is no control over the evolution of the maximal tree level difference $L_J$ and should not be employed directly if the flat top property is to be enforced globally by a level-dependent scaling parameter $\alpha_k \in (1, 1+2^{-L_k})$. To bound the constants in (8) uniformly it is necessary to limit the level-difference $L_k$ independently of the number of levels. This can be achieved by the cover smoothing scheme presented in [23] which can be easily incorporated into our hp-adaptive scheme.

### 3.3 Summary

For the sake of completeness let us summarize the computational steps of an hp-adaptive PPUM computation for the numerical treatment of our model problem (12). To this end let us assume that we already have a sequence of PPUM spaces $V_k^{\mathrm{PU}}$ with associated covers $C_\Omega^k$ and polynomial degrees

$$p_{\min,k} := \min_{i=1}^{N_k} p_{i,k}, \quad p_{\max,k} := \max_{i=1}^{N_k} p_{i,k} \tag{24}$$

for $k = 1, \ldots, J$ and predicted error values $\eta_{i,*}$ for $i = 1, \ldots, N_k$.

1. Estimate the global regularization parameter $\beta_J$ associated with the space $V_J^{\mathrm{PU}}$ employed in (13) via local eigenvalue problems corresponding to (17).
2. Discretize the weak form (14) with the estimated $\beta_J$ via Galerkin's method with the trial and test space $V_J^{\mathrm{PU}}$ using the basis functions $\varphi_{i,J}\psi_{i,J}^n$.
3. Solve the arising global linear system $A\tilde{u} = \hat{f}$ on level $J$ with a full multigrid solver [19, 23] based on the complete sequence $\{V_k^{\mathrm{PU}}\}_{k=1}^J$.
4. Define the local approximation spaces $V_{i,*} := \varphi_{i,J} V_{i,J}^{p_{i,J}+q}$ in (19) for the local error approximation.
5. Estimate the local regularization parameters $\beta_{i,*}$ associated with the space $V_{i,*}$ employed in (19) by a respective local eigenvalue problem corresponding to (17).
6. Discretize (19), i.e. (20), with the estimated $\beta_{i,*}$. Solve the local linear system $A_{i,*}\tilde{e}_{i,*} = \hat{r}_{i,*}$ using a direct solver.
7. Estimate the local errors $\eta_i$ and the global error $\eta$ with respect to the energy-norm $\|\cdot\|_{A,J}$ by (21).
8. Define the refinement indicator function (18) using the estimed local errors $\eta_i$ and the predicted error values $\eta_{i,*}$.
9. If $\eta > \epsilon_{\mathrm{tol}}$, refine the global PPUM space $V_J^{\mathrm{PU}}$ according to (18), define the new predicted errors $\eta_{i,*}$ with respect to $\|\cdot\|_{A,J}$ according to (22) and return to 1.

## 4 Numerical Results

In this section we present some results of our numerical experiments using the hp-adaptive PPUM discussed above. To this end, we introduce some shorthand notation for various norms of the error $u - u^{\mathrm{PU}}$, i.e., we define

$$e_{L^\infty} := \frac{\|u - u^{\mathrm{PU}}\|_{L^\infty}}{\|u\|_{L^\infty}}, e_{L^2} := \frac{\|u - u^{\mathrm{PU}}\|_{L^2}}{\|u\|_{L^2}}, e_{H^1} := \frac{\|\nabla(u - u^{\mathrm{PU}})\|_{L^2}}{\|\nabla u\|_{L^2}}. \tag{25}$$

Analogously, we introduce the notion

$$e^*_{H^1} := \frac{\eta_{H^1}}{\|\nabla u\|_{L^2}} = \frac{\left(\sum_{\omega_i \in C_\Omega} \eta^2_{i,H^1}\right)^{\frac{1}{2}}}{\|\nabla u\|_{L^2}} = \frac{\left(\sum_{\omega_i \in C_\Omega} \|\nabla e_{i,*}\|^2_{L^2}\right)^{\frac{1}{2}}}{\|\nabla u\|_{L^2}} \tag{26}$$

for the estimated (relative) error using (19) and (21). For each of these error norms we compute the respective algebraic convergence rate $\rho$ by considering the error norms of two consecutive levels $l-1$ and $l$

$$\rho := -\frac{\log\left(\frac{\|u-u^{\mathrm{PU}}_l\|}{\|u-u^{\mathrm{PU}}_{l-1}\|}\right)}{\log(\frac{\mathsf{dof}_l}{\mathsf{dof}_{l-1}})}, \quad \text{where } \mathsf{dof}_k := \sum_{i=1}^{N_k} \dim(V^{p_{i,k}}_{i,k}). \tag{27}$$

Hence the optimal rate $\rho_{H^1}$ of an h-refined space with $p_i = p$ is $\rho_{H^1} = \frac{p}{d}$ where $d$ denotes the space dimension of $\Omega \subset \mathbb{R}^d$.

Note that the definition of the relative error with respect to the energy-norm is not straightforward. This is due to the use of the cover-dependent scaling parameters $\gamma_{i,D}$ and the space-dependent regularization parameter $\beta$ in (13). Therefore the bilinear form (15) and the associated energy-norm are dependent on the employed discretization space so that we deal with a sequence of energy-norms $\|\cdot\|_{A,k} := \sqrt{a_k(\cdot,\cdot)}$ for $k = 1, \ldots, J$ and we define

$$e_{A,k} := \frac{\|u - u^{\mathrm{PU}}\|_{A,k}}{\|u\|_{A,0}} \tag{28}$$

where $\|\cdot\|_{A,0}$ denotes the classical energy-norm ignoring all additional surface terms due to Nitsche's method. The values $\rho_{A,k}$ now involve the two successive energy-norms $\|\cdot\|_{A,k}$ and $\|\cdot\|_{A,k-1}$. To assess the quality of our error estimator (21) we give its effectivity index with respect to the energy-norm

$$\epsilon^*_{A,k} := \frac{e^*_{A,k}}{e_{A,k}} = \frac{\eta_{A,k}}{\|(u - u^{\mathrm{PU}})\|_{A,k}}.$$

All these norms are approximated using a numerical integration scheme with very high resolution based on the finest refinement level.

In all our examples we used $q = 2$ for the estimation of the error via (19) and the values $\sigma_b = 0.8$, $\sigma_{\mathtt{null}} = 1$, $\sigma_{\mathtt{h}} = 3$, and $\sigma_{\mathtt{p}} = 0.6$, see (22), in the definition of the refinement indicator (18).

**Example 4.1** In the first example we apply our hp-adaptive PPUM to the model problem (12) with Dirichlet boundary conditions on an L-shaped domain $\Omega = (-1,1)^2 \setminus [0,1]^2$. We choose the data of the right-hand side such that the solution is given by

$$u(x,y) = u(r,\theta) = r^{\frac{2}{3}} \sin\left(\frac{2\theta - \pi}{3}\right).$$

In the hp-FEM [34] the optimal convergence behavior attainable for this type of problem is the exponential error bound

$$\|u - u^{\mathrm{PU}}\|_{H^1(\Omega)} \leq C \exp(-b\ \mathsf{dof}^{1/3}). \tag{29}$$

The measured errors (25) and respective convergence rates (27) are given in Table 1. Furthermore, we give the number of degrees of freedom $\mathsf{dof}$, the number of patches $N$, maximal tree level difference $L$, the range of employed polynomial degrees $[p] := [p_{\min}, p_{\max}]$, compare (24), for the respective level $J$.

We anticipate to find an exponential convergence of our hp-adaptive PPUM. Thus the algebraic convergence rates $\rho$ should increase with an increasing number of levels $J$. From the numbers given in Table 1 we can clearly observe this anticipated behavior. To assess the quality of our hp-adaptive PPUM discretization quantitatively we give a plot of the measured errors against $\mathsf{dof}^{1/3}$ in Figure 2. From the plots on the left of Figure 2 we can clearly observe a perfect agreement with the bound (29). Hence, our local error estimator $\eta_i$ (21) and the presented refinement indicator function $r$ (18) are very well suited and provide an optimal error reduction. This observation holds well up to refinement level $J = 19$ where $p_{\max} = 7$ and $L_J = 6$. On more refined levels $J > 19$ with $p_{\max} > 7$ and $L_J \geq 6$ we find a slight deterioration of this optimal behavior, see Figure 2 (right) and Table 1. This effect is (most probably) due to numerical integration errors. The employed subdivision sparse grid numerical integration scheme [18] employs quadrature rules that are exponentially convergent but have a multi-variate polynomial exactness of order 13 only. Hence, if we assume that the PU function is resolved by the employed subdivision for numerical integration, we can compute the entries of the stiffness matrix (almost) exactly for $p \leq 6$ only. The understanding of the effects of numerical integration in meshfree methods is rather involved and far from complete and a detailed study of the observed behavior is subject of current research. Note that we obtained similar results when we limit $L_J < 4$ globally so that the influence of the parameter $L_J$ on the convergence behavior is negligable.

In Figure 3 we give some snapshots of the distribution of the polynomial degrees on levels $J = 10, 13, 16$. From these plots, we can observe a linear increase in the polynomial degree towards the re-entrant corner and a substantial increase in the local refinement-level of the employed tree in the vicinity of the singularity. We can also see the large irregularity of the tree with $L_{16} = 4$ from these plots.

**Example 4.2** In our second example we consider our model problem (12) in three space dimensions on the domain $\Omega = (-1, 1)^3 \setminus [0, 1]^3$ with vanishing Dirichlet boundary conditions $g_D = 0$ and right-hand side $f = 1$. In this example we measure absolute errors only and we estimate the error $e^*_{L^2}$ with respect to the $L^2$-norm analogously to (26).

Table 1
Relative errors $e$ (25) and convergence rates $\rho$ (27) for Example 4.1.

| $J$ | dof | $N$ | $[p]$ | $L$ | $e_{L^\infty}$ | $\rho_{L^\infty}$ | $e_{L^2}$ | $\rho_{L^2}$ | $e_{H^1}$ | $\rho_{H^1}$ | $e_{A,J}$ | $\rho_{A,J}$ | $e^*_{A,J}$ | $\rho^*_{A,J}$ | $\epsilon^*_{A,J}$ |
|---|---|---|---|---|---|---|---|---|---|---|---|---|---|---|---|
| 3 | 144 | 48 | $[1,1]$ | 0 | $4.54_{-2}$ | 0.34 | $8.91_{-3}$ | 0.57 | $1.14_{-1}$ | 0.30 | $9.91_{-2}$ | 0.29 | $3.01_{-1}$ | 0.87 | 3.04 |
| 4 | 171 | 57 | $[1,1]$ | 1 | $2.85_{-2}$ | 2.71 | $5.62_{-3}$ | 2.68 | $8.95_{-2}$ | 1.42 | $8.24_{-2}$ | 1.07 | $2.26_{-1}$ | 1.67 | 2.74 |
| 5 | 216 | 72 | $[1,1]$ | 1 | $1.80_{-2}$ | 1.97 | $4.10_{-3}$ | 1.35 | $7.42_{-2}$ | 0.80 | $7.11_{-2}$ | 0.63 | $1.56_{-1}$ | 1.59 | 2.19 |
| 6 | 291 | 93 | $[1,2]$ | 1 | $1.13_{-2}$ | 1.56 | $2.50_{-3}$ | 1.66 | $5.74_{-2}$ | 0.86 | $5.59_{-2}$ | 0.81 | $1.09_{-1}$ | 1.21 | 1.94 |
| 7 | 414 | 120 | $[1,2]$ | 1 | $6.90_{-3}$ | 1.40 | $1.71_{-3}$ | 1.08 | $4.45_{-2}$ | 0.72 | $4.66_{-2}$ | 0.52 | $6.10_{-2}$ | 1.64 | 1.31 |
| 8 | 633 | 168 | $[1,2]$ | 1 | $4.39_{-3}$ | 1.06 | $6.86_{-4}$ | 2.15 | $2.54_{-2}$ | 1.32 | $2.65_{-2}$ | 1.33 | $3.46_{-2}$ | 1.34 | 1.31 |
| 9 | 874 | 207 | $[1,3]$ | 1 | $2.69_{-3}$ | 1.52 | $2.74_{-4}$ | 2.85 | $1.51_{-2}$ | 1.61 | $1.55_{-2}$ | 1.66 | $2.05_{-2}$ | 1.62 | 1.32 |
| 10 | 1279 | 282 | $[1,3]$ | 2 | $2.03_{-3}$ | 0.73 | $1.45_{-4}$ | 1.68 | $9.28_{-3}$ | 1.28 | $9.55_{-3}$ | 1.27 | $1.10_{-2}$ | 1.63 | 1.15 |
| 11 | 1791 | 345 | $[1,4]$ | 2 | $1.29_{-3}$ | 1.35 | $6.38_{-5}$ | 2.43 | $5.63_{-3}$ | 1.48 | $5.75_{-3}$ | 1.51 | $6.50_{-3}$ | 1.56 | 1.13 |
| 12 | 2620 | 501 | $[1,4]$ | 3 | $8.32_{-4}$ | 1.16 | $2.58_{-5}$ | 2.38 | $3.17_{-3}$ | 1.51 | $3.24_{-3}$ | 1.51 | $4.07_{-3}$ | 1.23 | 1.26 |
| 13 | 3324 | 612 | $[1,5]$ | 3 | $5.53_{-4}$ | 1.71 | $1.54_{-5}$ | 2.16 | $2.11_{-3}$ | 1.71 | $2.15_{-3}$ | 1.72 | $2.70_{-3}$ | 1.72 | 1.26 |
| 14 | 4884 | 882 | $[1,5]$ | 4 | $3.49_{-4}$ | 1.20 | $8.22_{-6}$ | 1.63 | $1.39_{-3}$ | 1.09 | $1.41_{-3}$ | 1.10 | $1.73_{-3}$ | 1.15 | 1.23 |
| 15 | 6653 | 1236 | $[1,5]$ | 4 | $2.19_{-4}$ | 1.51 | $4.33_{-6}$ | 2.07 | $8.33_{-4}$ | 1.65 | $8.51_{-4}$ | 1.64 | $9.34_{-4}$ | 2.00 | 1.10 |
| 16 | 9059 | 1620 | $[1,6]$ | 4 | $1.42_{-4}$ | 1.40 | $1.55_{-6}$ | 3.32 | $5.31_{-4}$ | 1.46 | $5.40_{-4}$ | 1.47 | $6.13_{-4}$ | 1.36 | 1.14 |
| 17 | 12472 | 2349 | $[1,6]$ | 5 | $8.99_{-5}$ | 1.43 | $8.81_{-7}$ | 1.78 | $3.13_{-4}$ | 1.65 | $3.19_{-4}$ | 1.65 | $3.62_{-4}$ | 1.64 | 1.14 |
| 18 | 16117 | 2862 | $[1,7]$ | 5 | $5.69_{-5}$ | 1.78 | $4.64_{-7}$ | 2.50 | $2.14_{-4}$ | 1.49 | $2.17_{-4}$ | 1.50 | $2.37_{-4}$ | 1.65 | 1.09 |
| 19 | 23145 | 4458 | $[1,7]$ | 6 | $3.73_{-5}$ | 1.17 | $2.86_{-7}$ | 1.34 | $1.25_{-4}$ | 1.47 | $1.28_{-4}$ | 1.46 | $1.28_{-4}$ | 1.70 | 1.00 |
| 20 | 30046 | 5415 | $[1,8]$ | 6 | $2.41_{-5}$ | 1.67 | $9.62_{-8}$ | 4.17 | $8.48_{-5}$ | 1.50 | $8.63_{-5}$ | 1.51 | $8.45_{-5}$ | 1.60 | 0.98 |
| 21 | 45724 | 8925 | $[1,8]$ | 7 | $1.52_{-5}$ | 1.09 | $6.13_{-8}$ | 1.07 | $4.76_{-5}$ | 1.38 | $4.87_{-5}$ | 1.36 | $4.74_{-5}$ | 1.38 | 0.97 |
| 22 | 56520 | 10707 | $[1,9]$ | 7 | $9.60_{-6}$ | 2.18 | $2.78_{-8}$ | 3.72 | $3.25_{-5}$ | 1.80 | $3.32_{-5}$ | 1.82 | $3.20_{-5}$ | 1.85 | 0.97 |
| 23 | 83021 | 16683 | $[1,9]$ | 7 | $6.28_{-6}$ | 1.10 | $1.86_{-8}$ | 1.04 | $1.93_{-5}$ | 1.36 | $1.99_{-5}$ | 1.32 | $1.81_{-5}$ | 1.49 | 0.91 |
| 24 | 107269 | 21180 | $[1,10]$ | 8 | $3.96_{-6}$ | 1.80 | $7.16_{-9}$ | 3.73 | $1.25_{-5}$ | 1.71 | $1.29_{-5}$ | 1.71 | $1.16_{-5}$ | 1.73 | 0.90 |
| 25 | 154450 | 31041 | $[1,10]$ | 8 | $2.49_{-6}$ | 1.27 | $3.17_{-9}$ | 2.24 | $7.51_{-6}$ | 1.39 | $7.77_{-6}$ | 1.38 | $6.97_{-6}$ | 1.39 | 0.90 |
| 26 | 198786 | 41091 | $[1,11]$ | 9 | $1.57_{-6}$ | 1.83 | $1.93_{-9}$ | 1.96 | $4.72_{-6}$ | 1.84 | $4.87_{-6}$ | 1.85 | | | |

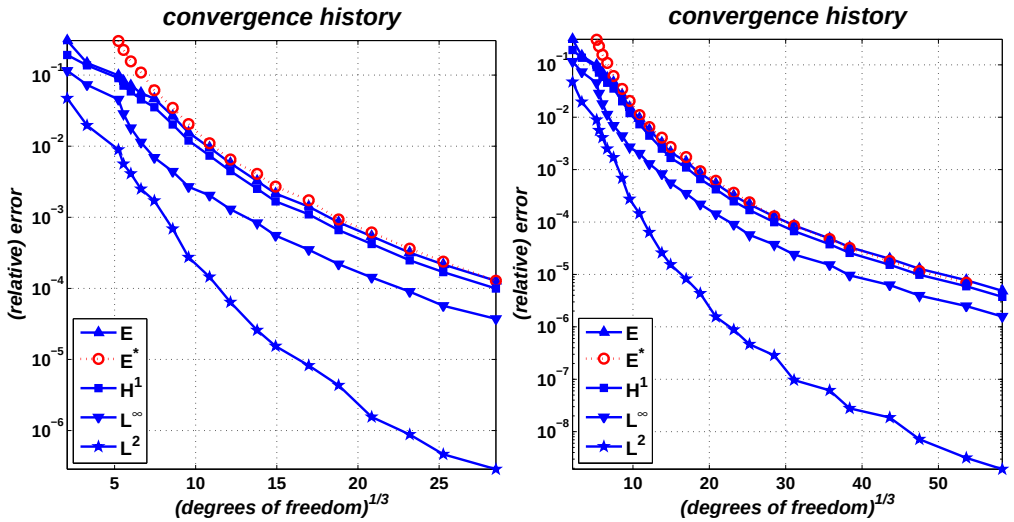


Figure 2. Convergence history of the measured relative errors $e$ (25) in the $L^\infty$-norm, the $L^2$-norm, the $H^1$-seminorm, and the energy-norm on the respective level (denoted by $E$ in the legend) for Example 4.1. The dotted red line with circular markers gives the estimated error (21) (denoted by $E^*$ in the legend) used to steer the refinement process. On the left are the results up to level $J = 19$, on the right up to level 26.

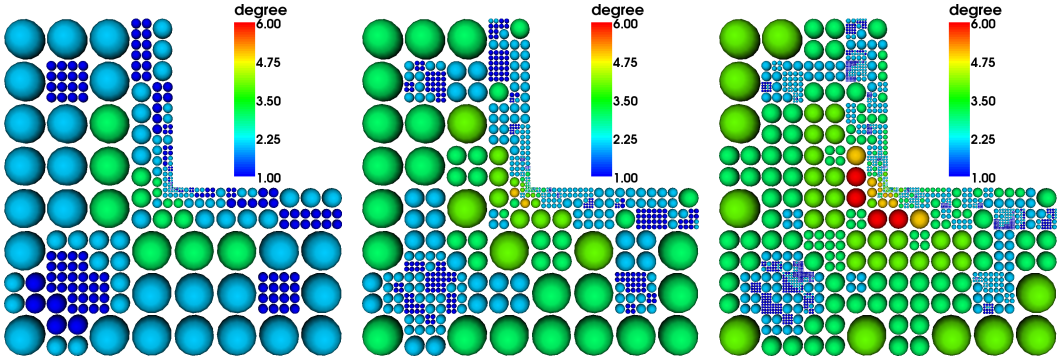


Figure 3. Depicted is the distribution of the polynomial degrees for levels $J = 10, 13, 16$ (left to right) for Example 4.1 on the cell centers of the respective tree decomposition. The size of the particle at the cell center indicates the size of the respective support patch, the color of the particle indicates the employed polynomial degree on the patch.

Table 2
Estimated errors $e^*$ (26) and respective convergence rates $\rho^*$ (27) for Example 4.2.

| $J$ | dof | $N$ | $[p]$ | $L_C$ | $e^*_{L^2}$ | $\rho^*_{L^2}$ | $e^*_{H^1}$ | $\rho^*_{H^1}$ | $e^*_{A,J}$ | $\rho^*_{A,J}$ |
|---|---|---|---|---|---|---|---|---|---|---|
| 3 | 1792 | 448 | $[1,1]$ | 0 | $6.673_{-3}$ | 0.55 | $2.315_{-1}$ | 0.24 | $3.475_{-1}$ | 0.30 |
| 4 | 14336 | 3584 | $[1,1]$ | 0 | $1.881_{-3}$ | 0.61 | $1.280_{-1}$ | 0.28 | $1.721_{-1}$ | 0.34 |
| 5 | 58996 | 14749 | $[1,1]$ | 1 | $1.174_{-3}$ | 0.33 | $9.464_{-2}$ | 0.21 | $1.072_{-1}$ | 0.33 |
| 6 | 131366 | 28091 | $[1,2]$ | 1 | $3.085_{-4}$ | 1.67 | $4.446_{-2}$ | 0.94 | $5.292_{-2}$ | 0.88 |
| 7 | 276180 | 47166 | $[1,3]$ | 2 | $8.861_{-5}$ | 1.68 | $2.059_{-2}$ | 1.04 | $2.390_{-2}$ | 1.07 |
| 8 | 659599 | 109291 | $[1,4]$ | 2 | $7.210_{-5}$ | 0.24 | $1.622_{-2}$ | 0.27 | $2.038_{-2}$ | 0.18 |
| 9 | 1468658 | 220969 | $[1,5]$ | 3 | $2.430_{-5}$ | 1.36 | $9.816_{-3}$ | 0.63 | $1.324_{-2}$ | 0.54 |

The estimated errors $e^*$ and the respective convergence rates $\rho^*$ are given in Table 2. Again, we can observe and increase in the rates $\rho^*$ for increasing refinement levels $J$ indicating an exponential convergence. In Figure 4 we plotted the estimated errors against $\mathsf{dof}^{1/5}$. From these graphs we see that the convergence behavior is very close to the optimal hp-FEM behavior for this problem.

**Example 4.3** In our last example, we consider a reference problem from linear elastic fracture mechanics.

$$\begin{aligned} -\operatorname{\mathbf{div}} \boldsymbol{\sigma}(u) &= f \quad \text{in } \Omega = (-1,1)^2, \\ \boldsymbol{\sigma}(u) \cdot n &= g_N \text{ on } \Gamma_N \subset \partial\Omega \cup C, \\ u &= g_D \text{ on } \Gamma_D = \partial\Omega \setminus \Gamma_N, \end{aligned} \tag{30}$$

with material parameters $E = 1$ and $\nu = 0.3$. The Dirichlet boundary is given by $\Gamma_D := \{(x,y) \in \partial\Omega \,|\, y = -1\}$ and we use $g_D = (0,0)$. On the upper boundary $\{(x,y) \in \partial\Omega \,|\, y = 1\} \subset \Gamma_N$ we use $g_N = (0,1)$. On the remaining parts of the Neumann boundary $\Gamma_N$ we use $g_N = (0,0)$. The internal traction-free segment

$$C := \{(x,y) \in \Omega \,|\, x \in (0.25, 0) \text{ and } y = 0\}$$

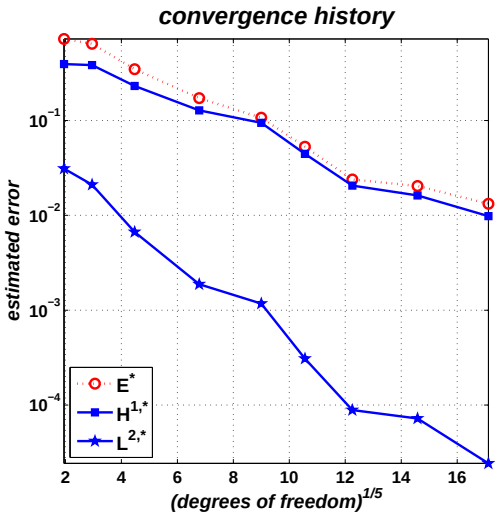


Figure 4. Convergence history of the estimated errors $e^*$ (26) with respect to the $L^2$-norm, the $H^1$-seminorm, and the energy-norm on the respective level (denoted by $E$ in the legend) for Example 4.2.

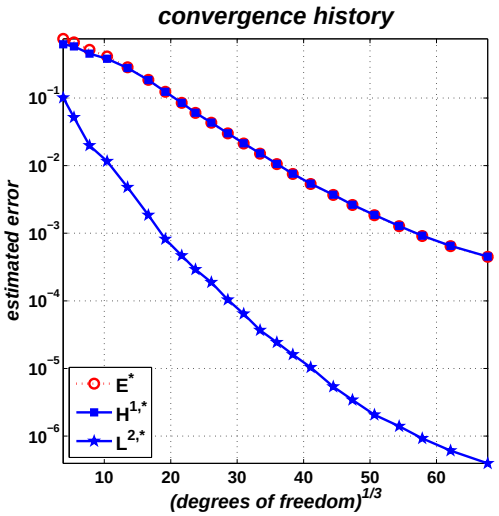


Figure 5. Convergence history of the estimated errors $e^*$ (26) with respect to the $L^2$-norm, the strain energy-seminorm (denoted by $H^1$ in the legend), and the energy-norm on the respective level (denoted by $E$ in the legend) for Example 4.3.

is referred to as a crack. The crack $C$ induces a discontinuous displacement field $u$ across the crack line with singularities at the crack tips $c_l := (0.25, 0)$ and $c_u := (0.75, 0)$. Hence, the local approximation spaces employed in our PPUM must respect these features to provide good approximation. Therefore, a crack tip is modeled by special analytical enrichment functions $\zeta^m$

$$\{\zeta^m_{\text{tip}}\} := \{\sqrt{r}\cos\frac{\theta}{2}, \sqrt{r}\sin\frac{\theta}{2}, \sqrt{r}\sin\theta\sin\frac{\theta}{2}, \sqrt{r}\sin\theta\cos\frac{\theta}{2}\}$$

with respect to a local polar coordinate system centered in the respective crack tip. The discontinuous part is modeled by $\{\zeta^m_{\text{jump},i}\} := s_{\pm,i} H_C V^{p_{i,k}}_{i,k}$ where $s_{\pm,i} > 0$ denotes two local scaling parameters, and $H_C$ refers to the Haar function. The scaling parameters $s_{\pm,i}$ are chosen based on $\mu(\{H_C \equiv 1\} \cap \omega_i)$ and $\mu(\{H_C \equiv -1\} \cap \omega_i)$ to control the conditioning of the local basis. This approach is similar to the enrichment techniques employed in other meshfree methods e.g. [7, 31], the generalized finite element method [13, 14], and the extended finite element method [6, 8, 29].

In this paper we employ a minimal enrichment criterion only, i.e., we use the

local approximation spaces

$$V_{i,k}^{p_{i,k}} := \begin{cases} \mathcal{P}^{p_{i,k}} \circ T_{i,k} & \text{if } \omega_{i,k} \cap C = \emptyset, \\ \mathcal{P}^{p_{i,k}} \circ T_{i,k} \oplus \{\zeta_{c_l}^m\} & \text{else if } c_l \in \omega_{i,k}, \\ \mathcal{P}^{p_{i,k}} \circ T_{i,k} \oplus \{\zeta_{c_u}^m\} & \text{else if } c_u \in \omega_{i,k}, \\ \mathcal{P}^{p_{i,k}} \circ T_{i,k} \oplus s_{\pm,i} H_C \mathcal{P}^{p_{i,k}} \circ T_{i,k} & \text{else.} \end{cases} \tag{31}$$

Note that there is a fundamental difference in the singular enrichment at the crack tips compared with the discontinuous enrichment at the crack line. The tip enrichment is additive and increases the local dimension by a constant $\dim(V_{i,k}^{p_{i,k}}) = \dim(\mathcal{P}^{p_{i,k}}) + 4$ only. The discontinuous enrichment is multiplicative and doubles the dimension of the local polynomial space, i.e., $\dim(V_{i,k}^{p_{i,k}}) = 2\ \dim(\mathcal{P}^{p_{i,k}})$.

In this example we measure absolute errors only and use the strain energy seminorm $\|\boldsymbol{\epsilon}(u)\|_{L^2(\Omega)} = \|\frac{1}{2}(\boldsymbol{\nabla}(u) + \boldsymbol{\nabla}^T(u))\|_{L^2(\Omega)}$ for the definition of $e_{H^1}^*$ of (26). The estimated errors $e_{A,J}^*$, $e_{H^1}^*$, and $e_{L^2}^*$ and the respective convergence rates $\rho^*$ are given in Table 3. From these numbers we can observe an increase of the algebraic rates $\rho$ which corresponds to an exponential convergence of the approximation. In Figure 5 we have plotted the estimated errors against $\mathsf{dof}^{1/3}$ and obtain (almost) straight lines indicating also in this example an error bound of type (29).

In Figure 6 we plotted the mode I stress intensity factor (SIF) of the upper crack tip $c_u$ against the refinement level and in Figure 7 against the employed extraction radius using the contour integral method [44]. Note that we employ square extraction domains centered in $c_u$ with arbitrary radii that do not align with the support patches. From these plots we can clearly observe the path independence for a very large range of extraction radii—virtually constant extraction values from $10^0$ down to $10^{-3}$ and only very small oscillations for radii between $10^{-3}$ and $10^{-6}$—as well as the fast convergence of the SIF. Finally, we give snapshots of the distribution of the employed polynomial degrees on the (scaled) deformed configuration in Figure 8 and for the distribution of the von Mises stress in Figure 9. From these plots, we clearly see the hp-adaptive resolution of the singularities near the crack tips as well as the additional singularities in the Dirichlet-Neumann corners. Note also that across the crack line we obtain a (pure) p-refinement in regions where the displacement field is locally (above/below the crack line) smooth. We attain this optimal behavior due to the choice of a multiplicative enrichment across the crack line.

**Remark 4.1** Note that for the employed analytical enrichment we need to assume that the curvature of the crack line near the crack tip is completely resolved by the cover patches (h-refinement) so that the transformation to polar coordinates is sensible. Another approach which is more in the spirit of

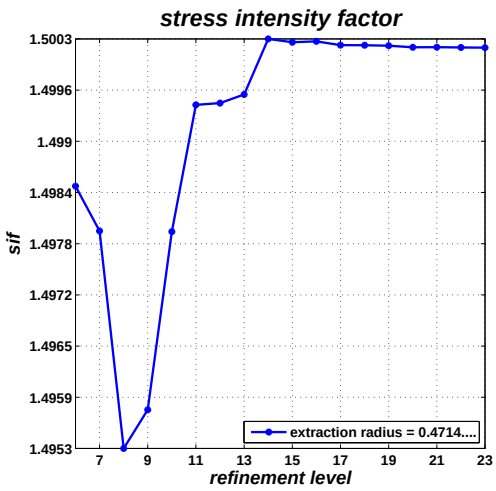


Figure 6. The convergence history for the mode I stress intensity factor of the upper crack tip $c_u$ for Example 4.3 with respect to the refinement levels.

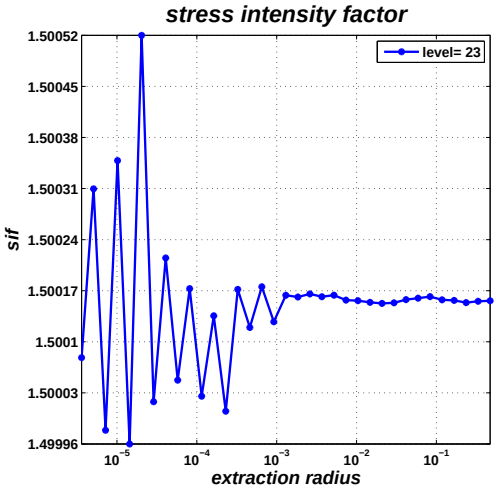


Figure 7. The path independence of the extracted mode I stress intensity factor of the upper crack tip $c_u$ for Example 4.3.

Table 3
Estimated errors $e^*$ (26) and respective convergence rates $\rho^*$ (27) for Example 4.3.

| $J$ | dof | $N$ | $[p]$ | $L_{\mathcal{C}}$ | $e^*_{L^2}$ | $\rho^*_{L^2}$ | $e^*_{H^1}$ | $\rho^*_{H^1}$ | $e^*_{A,J}$ | $\rho^*_{A,J}$ |
|---|---|---|---|---|---|---|---|---|---|---|
| 3 | 472 | 64 | $[1,1]$ | 0 | $1.981_{-2}$ | 0.89 | $4.530_{-1}$ | 0.23 | $5.164_{-1}$ | 0.23 |
| 4 | 1132 | 166 | $[1,1]$ | 1 | $1.159_{-2}$ | 0.61 | $3.805_{-1}$ | 0.20 | $4.120_{-1}$ | 0.26 |
| 5 | 2464 | 346 | $[1,2]$ | 2 | $4.782_{-3}$ | 1.14 | $2.777_{-1}$ | 0.41 | $2.852_{-1}$ | 0.47 |
| 6 | 4600 | 568 | $[1,3]$ | 2 | $1.851_{-3}$ | 1.52 | $1.846_{-1}$ | 0.65 | $1.860_{-1}$ | 0.68 |
| 7 | 7068 | 778 | $[1,3]$ | 2 | $8.175_{-4}$ | 1.90 | $1.237_{-1}$ | 0.93 | $1.238_{-1}$ | 0.95 |
| 8 | 10144 | 1066 | $[1,3]$ | 3 | $4.676_{-4}$ | 1.55 | $8.485_{-2}$ | 1.04 | $8.494_{-2}$ | 1.04 |
| 9 | 13364 | 1330 | $[1,4]$ | 3 | $2.914_{-4}$ | 1.72 | $6.044_{-2}$ | 1.23 | $6.020_{-2}$ | 1.25 |
| 10 | 17800 | 1708 | $[1,4]$ | 3 | $1.879_{-4}$ | 1.53 | $4.332_{-2}$ | 1.16 | $4.310_{-2}$ | 1.17 |
| 11 | 23380 | 2140 | $[1,4]$ | 4 | $1.036_{-4}$ | 2.18 | $3.014_{-2}$ | 1.33 | $3.001_{-2}$ | 1.33 |
| 12 | 29716 | 2608 | $[1,4]$ | 4 | $6.432_{-5}$ | 1.99 | $2.138_{-2}$ | 1.43 | $2.124_{-2}$ | 1.44 |
| 13 | 37412 | 3160 | $[1,5]$ | 4 | $3.680_{-5}$ | 2.42 | $1.518_{-2}$ | 1.49 | $1.504_{-2}$ | 1.50 |
| 14 | 46536 | 3922 | $[1,5]$ | 4 | $2.431_{-5}$ | 1.90 | $1.061_{-2}$ | 1.64 | $1.055_{-2}$ | 1.63 |
| 15 | 56476 | 4582 | $[1,6]$ | 5 | $1.605_{-5}$ | 2.14 | $7.583_{-3}$ | 1.73 | $7.525_{-3}$ | 1.74 |
| 16 | 69256 | 5542 | $[1,6]$ | 5 | $1.037_{-5}$ | 2.14 | $5.405_{-3}$ | 1.66 | $5.357_{-3}$ | 1.67 |
| 17 | 87896 | 6856 | $[1,6]$ | 5 | $5.370_{-6}$ | 2.76 | $3.709_{-3}$ | 1.58 | $3.682_{-3}$ | 1.57 |
| 18 | 106188 | 7726 | $[1,6]$ | 5 | $3.421_{-6}$ | 2.39 | $2.640_{-3}$ | 1.80 | $2.616_{-3}$ | 1.81 |
| 19 | 129972 | 9424 | $[1,7]$ | 6 | $2.065_{-6}$ | 2.50 | $1.866_{-3}$ | 1.72 | $1.849_{-3}$ | 1.72 |
| 20 | 160800 | 11194 | $[1,7]$ | 6 | $1.396_{-6}$ | 1.84 | $1.281_{-3}$ | 1.77 | $1.272_{-3}$ | 1.76 |
| 21 | 193736 | 12826 | $[1,7]$ | 6 | $9.238_{-7}$ | 2.22 | $9.190_{-4}$ | 1.78 | $9.114_{-4}$ | 1.79 |
| 22 | 239784 | 15850 | $[1,7]$ | 6 | $6.079_{-7}$ | 1.96 | $6.501_{-4}$ | 1.62 | $6.445_{-4}$ | 1.62 |
| 23 | 310348 | 19648 | $[1,8]$ | 7 | $3.949_{-7}$ | 1.67 | $4.514_{-4}$ | 1.41 | $4.478_{-4}$ | 1.41 |

the PU technique is to design numerical enrichment functions [41, 42] using a local approximation near the crack tip [12, 37] which deals with the curvature of the crack line by the presented hp-adaptive technique. Furthermore, the approximation properties of an hp-refined PPUM space with enrichment can be further improved by employing an automatic multilevel enrichment control which allows refined patches to reuse the enrichment functions of a coarser patch [38] for approximation without compromising the stability of the global basis.

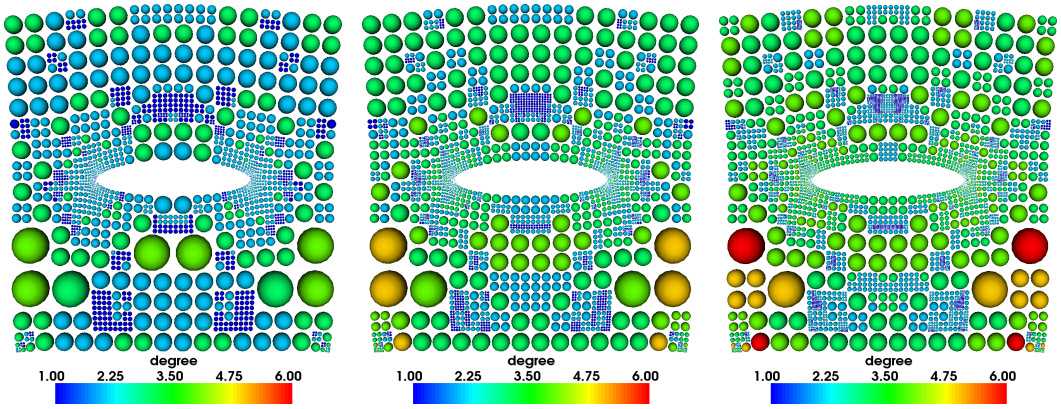


Figure 8. Depicted is the distribution of the polynomial degrees for levels $k = 10, 13, 16$ (left to right) for Example 4.3 on the cell centers of the respective deformed tree decomposition. The size of the particle at the cell center indicates the size of the respective support patch, the color of the particle indicates the employed polynomial degree on the patch.

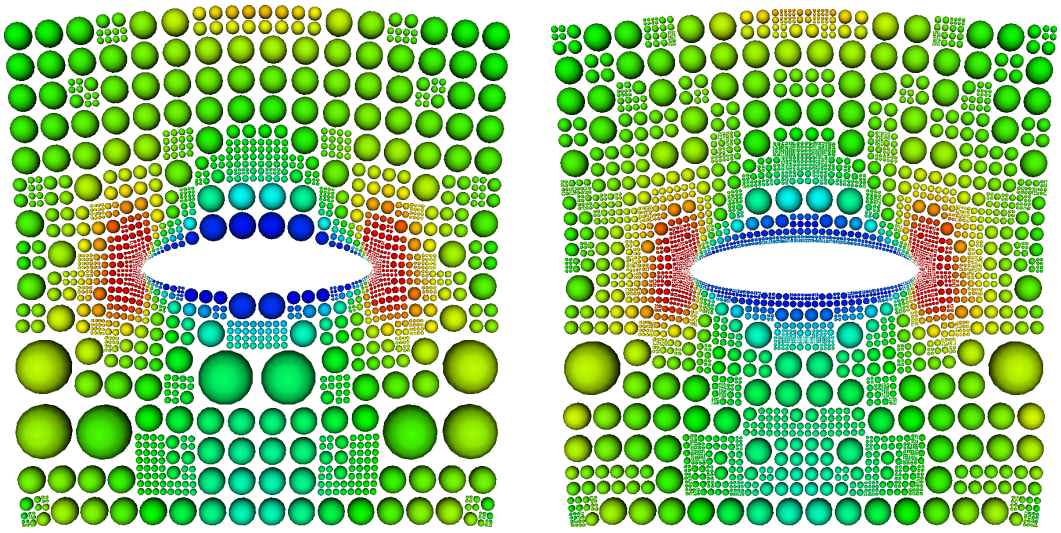

Figure 9. Depicted is the distribution of the von Mises stress for Example 4.3 on the cell centers of the respective deformed tree decomposition for levels $J = 10$ (left) and $J = 19$ (right). The size of the particle at the cell center indicates the size of the respective support patch, the color of the particle indicates the von Mises stress at the cell center.

## 5 Conclusion

In this paper we presented an hp-adaptive version of our multilevel PPUM for the efficient numerical treatment of second order elliptic PDEs. The proposed scheme employs a sub-domain error estimator and a one-level history to steer the refinement process. The overall goal of the PPUM approach is not only to employ a classical hp-type discretization but to use more sophisticated enrichment functions to deal with particular local features of the solution. The

developed hp-adaptive PPUM is designed to serve as a basis for the automatic approximation of such singular enrichment functions.

The results of our numerical experiments in two and three dimensions (including analytical enrichment functions) clearly demonstrate the exponential convergence behavior of our PPUM for problems with singular solutions. This renders our hp-adaptive PPUM applicable for the automatic construction of numerical enrichment functions for instance in the case of curved cracks.

## References


[1] I. Babuška, U. Banerjee, and J. E. Osborn, *Survey of Meshless and Generalized Finite Element Methods: A Unified Approach*, Acta Numerica, (2003), pp. 1–125.

[2] I. Babuška, G. Caloz, and J. E. Osborn, *Special Finite Element Methods for a Class of Second Order Elliptic Problems with Rough Coefficients*, SIAM J. Numer. Anal., 31 (1994), pp. 945–981.

[3] I. Babuška and J. M. Melenk, *The Partition of Unity Method*, Int. J. Numer. Meth. Engrg., 40 (1997), pp. 727–758.

[4] I. Babuška and W. C. Rheinboldt, *Error Estimates for Adaptive Finite Element Computations*, SIAM J. Numer. Anal., 15 (1978), pp. 736–754.

[5] S. Beissel and T. Belytschko, *Nodal Integration of the Element-Free Galerkin Method*, Comput. Meth. Appl. Mech. Engrg., 139 (1996), pp. 49–74.

[6] T. Belytschko and T. Black, *Elastic crack growth in finite elements with minimal remeshing*, Int. J. Numer. Meth. Engrg., 45 (1999), pp. 601–620.

[7] T. Belytschko, Y. Y. Lu, and L. Gu, *Crack propagation by element-free galerkin methods*, Engrg. Frac. Mech., 51 (1995), pp. 295–315.

[8] T. Belytschko, N. Moës, S. Usui, and C. Parimi, *Arbitrary discontinuities in finite elements*, Int. J. Numer. Meth. Engrg., 50 (2001), pp. 993–1013.

[9] J. S. Chen, C. T. Wu, and S. Yoon, *Non-linear Version of Stabilized Conforming Nodal Integration for Galerkin Mesh-free Methods*, Int. J. Numer. Meth. Engrg., 53 (2002), pp. 2587–2615.

[10] J. S. Chen, C. T. Wu, S. Yoon, and Y. You, *A Stabilized Conforming Nodal Integration for Galerkin Mesh-free Methods*, Int. J. Numer. Meth. Engrg., 50 (2001), pp. 435–466.

[11] J. Dolbow and T. Belytschko, *Numerical Integration of the Galerkin Weak Form in Meshfree Methods*, Comput. Mech., 23 (1999), pp. 219–230.

[12] C. A. Duarte and D.-J. Kim, *Analysis and applications of a generalized finite element method with global-local enrichment functions*, Comput. Meth. Appl. Mech. Engrg., (2007). to appear.

[13] C. A. M. Duarte, I. Babuška, and J. T. Oden, *Generalized Finite Element Methods for Three Dimensional Structural Mechanics Problems*, Comput. Struc., 77 (2000), pp. 215–232.

[14] C. A. M. Duarte, O. N. H. T. J. Liszka, and W. W. Tworzydlo, *A generalized finite element method for the simulation of three-dimensional dynamic crack propagation*, Int. J. Numer. Meth. Engrg., 190 (2001), pp. 2227–2262.

[15] C. A. M. Duarte and J. T. Oden, *hp Clouds – A Meshless Method to Solve Boundary Value Problems*, Numer. Meth. for PDE, 12 (1996), pp. 673–705.

[16] M. Griebel, P. Oswald, and M. A. Schweitzer, *A Particle-Partition of Unity Method—Part VI: A p-robust Multilevel Preconditioner*, in Meshfree Methods for Partial Differential Equations II, M. Griebel and M. A. Schweitzer, eds., vol. 43 of Lecture Notes in Computational Science and Engineering, Springer, 2005, pp. 71–92.

[17] M. Griebel and M. A. Schweitzer, *A Particle-Partition of Unity Method for the Solution of Elliptic, Parabolic and Hyperbolic PDE*, SIAM J. Sci. Comput., 22 (2000), pp. 853–890.

[18] ——, *A Particle-Partition of Unity Method—Part II: Efficient Cover Construction and Reliable Integration*, SIAM J. Sci. Comput., 23 (2002), pp. 1655–1682.

[19] ——, *A Particle-Partition of Unity Method—Part III: A Multilevel Solver*, SIAM J. Sci. Comput., 24 (2002), pp. 377–409.

[20] ——, *A Particle-Partition of Unity Method—Part V: Boundary Conditions*, in Geometric Analysis and Nonlinear Partial Differential Equations, S. Hildebrandt and H. Karcher, eds., Springer, 2002, pp. 517–540.

[21] ——, eds., *Meshfree Methods for Partial Differential Equations*, vol. 26 of Lecture Notes in Computational Science and Engineering, Springer, 2002.

[22] ——, eds., *Meshfree Methods for Partial Differential Equations II*, vol. 43 of Lecture Notes in Computational Science and Engineering, Springer, 2005.

[23] ——, *A Particle-Partition of Unity Method—Part VII: Adaptivity*, in Meshfree Methods for Partial Differential Equations III, M. Griebel and M. A. Schweitzer, eds., vol. 57 of Lecture Notes in Computational Science and Engineering, Springer, 2006, pp. 121–148.

[24] ——, eds., *Meshfree Methods for Partial Differential Equations III*, vol. 57 of Lecture Notes in Computational Science and Engineering, Springer, 2006.

[25] W. Hackbusch, *Multi-Grid Methods and Applications*, vol. 4 of Springer Series in Computational Mathematics, Springer, 1985.

[26] A. Huerta, T. Belytschko, T. Fernández-Méndez, and T. Rabczuk, *Meshfree Methods*, vol. 1 of Encyclopedia of Computational Mechanics, 2004, ch. 10, pp. 279–309.

[27] Y. Krongauz and T. Belytschko, *Enforcement of Essential Boundary Conditions in Meshless Approximations using Finite Elements*, Comput. Meth. Appl. Mech. Engrg., 131 (1996), pp. 133–145.

[28] J. M. Melenk and B. Wohlmuth, *On residual-based aposteriori error estimation in hp-FEM*, Adv. Comput. Math., 15 (2001), pp. 311–331.

[29] N. Moës, J. Dolbow, and T. Belytschko, *A finite element method for crack growth without remeshing*, Int. J. Numer. Meth. Engrg., 46 (1999), pp. 131–150.

[30] J. Nitsche, *Über ein Variationsprinzip zur Lösung von Dirichlet-Problemen bei Verwendung von Teilräumen, die keinen Randbedingungen unterworfen sind*, Abh. Math. Sem. Univ. Hamburg, 36 (1970–1971), pp. 9–15.

[31] J. T. Oden and C. A. Duarte, *Clouds, Cracks and FEM's*, 1997, pp. 302–321.

[32] N. Parés, P. Díez, and A. Huerta, *Subdomain-based flux-free a posteriori error estimators*, Comput. Meth. Appl. Mech. Engrg., 195 (2006), pp. 297–323.

[33] M. Puso, E. Zywicz, and J. S. Chen, *A new stabilized nodal integration approach*, in Meshfree Methods III, M. Griebel and M. A. Schweitzer, eds., Lecture Notes in Computational Science and Engineering, Springer, 2006, pp. 207–218.

[34] C. Schwab, *p- and hp-Finite Element Methods*, Clarendon Press, 1998.

[35] M. A. Schweitzer, *A Parallel Multilevel Partition of Unity Method for Elliptic Partial Differential Equations*, Dissertation, Institut für Angewandte Mathematik, Universität Bonn, 2002.

[36] ——, *A Parallel Multilevel Partition of Unity Method for Elliptic Partial Differential Equations*, vol. 29 of Lecture Notes in Computational Science and Engineering, Springer, 2003.

[37] ——, *Automatic dictionary assembly for the multilevel enrichment of the particle–partition of unity method*, tech. rep., Sonderforschungsbereich 611, Rheinische Friedrich-Wilhelms-Univeristät Bonn, 2007. in preparation.

[38] ——, *Automatic multilevel enrichment in the particle–partition of unity method*, tech. rep., Sonderforschungsbereich 611, Rheinische Friedrich-Wilhelms-Univeristät Bonn, 2007. in preparation.

[39] T. Strouboulis, I. Babuška, and K. Copps, *The Design and Analysis of the Generalized Finite Element Method*, Comput. Meth. Appl. Mech. Engrg., 181 (2000), pp. 43–69.

[40] T. Strouboulis, K. Copps, and I. Babuška, *The Generalized Finite Element Method*, Comput. Meth. Appl. Mech. Engrg., 190 (2001), pp. 4081–4193.

[41] T. Strouboulis, L. Zhang, and I. Babuška, *Generalized finite element method using mesh-based handbooks: Application to problems in domains with many voids*, Comput. Meth. Appl. Mech. Engrg., 192 (2003), pp. 3109–3161.

[42] ——, *p-version of the generalized fem using mesh-based handbooks with applications to multiscale problems*, 60 (2004), pp. 1639–1672.

[43] T. Strouboulis, L. Zhang, D. Wang, and I. Babuška, *A posteriori error estimation for generalized finite element methods*, Comput. Meth. Appl. Mech. Engrg., 195 (2006), pp. 852–879.

[44] B. Szabó and I. Babuška, *Finite Element Analysis*, John Wiley & Sons, 1991.

[45] J. Xu, *Iterative Methods by Space Decomposition and Subspace Correction*, SIAM Review, 34 (1992), pp. 581–613.